Hetero Bis-Addition of Spiro-Acetalized or Cyclohexanone Ring to 58π Fullerene Impacts Solubility and Mobility Balance in Polymer Solar Cells

Tsubasa Mikie,[†,‡] Akinori Saeki,* Naohiko Ikuma, Ken Kokubo,* and Shu Seki*[,†]

Department of Applied Chemistry, Graduate School of Engineering, Osaka University, 2-1 Yamadaoka, Suita, Osaka 565-0871, Japan

Ⓢ *Supporting Information*

ABSTRACT: Fullerene bis-adducts are increasingly being studied to gain a high open circuit voltage (V_{oc}) in bulk heterojunction organic photovoltaics (OPVs). We designed and synthesized homo and hetero bis-adduct [60]fullerenes by combining fused cyclohexanone or a five-membered spiro-acetalized unit (SAF$_5$) with 1,2-dihydromethano (CH$_2$), indene, or [6,6]-phenyl-C$_{61}$-butyric acid methyl ester (PCBM). These new eight 56π fullerenes showed a rational rise of the lowest unoccupied molecular orbital (LUMO). We perform a systematic study on the electrochemical property, solubility, morphology, and space-charge-limited current (SCLC) mobility. The best power conversion efficiency (PCE) of 4.43% (average, 4.36%) with the V_{oc} of 0.80 V was obtained for poly(3-hexylthiophene) (P3HT) blended with SAF$_5$/indene hetero bis-adduct, which is a marked advancement in PCE compared to the 0.9% of SAF$_5$ monoadduct. More importantly, we elucidate an important role of mobility balance between hole and electron that correlates with the device PCEs. Besides, an empirical equation to extrapolate the solubilities of hetero bis-adducts is proposed on the basis of those of counter monoadducts. Our work offers a guide to mitigate barriers for exploring a large number of hetero bis-adduct fullerenes for efficient OPVs.

KEYWORDS: *solubility, organic photovoltaic, fullerene bis-adduct, space-charge-limited current, mobility, bulk heterojunction, poly(3-hexylthiophene), regioisomers*
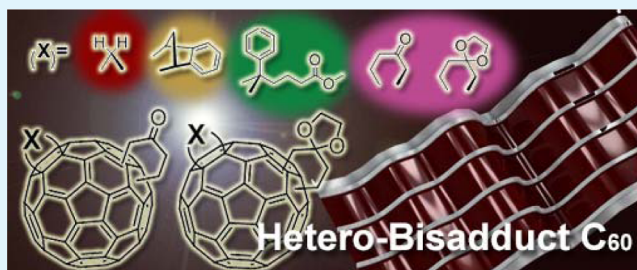
INTRODUCTION

Designing new conjugated polymers and fullerenes has been a vital theme with an ongoing strive toward highly efficient, lightweight, and low-cost organic photovoltaic (OPV) cells.[1−3] The continuing development from the early benchmark of regioregular poly(3-hexylthiophene) (P3HT) and PCBM[4−6] to low-bandgap polymers (LBPs)[7−10] has pushed the power conversion efficiencies (PCEs) to the respectful records of 9−10% for single cells.[11−15] In the high-performing tandem cells (PCEs, 9−11%),[16−18] P3HT or LBP blended with a soluble fullerene is used as the visible-light-absorbing top layer, where the shallow lowest unoccupied molecular orbital (LUMO) of fullerene is essential for a high open circuit voltage (V_{oc}).[19]

Multiaddition of substituent to a fullerene is hitherto among the most effective strategy for raising the LUMO level via symmetry break. For instance, Blom et al. reported that P3HT:bisPCBM exhibited a 0.15 V higher V_{oc} (0.73 V) than that of P3HT:PCBM, resulting in the improved PCE of 4.5%.[20] More recently, indene C$_{60}$ bis-adduct (ICBA) and other bis-adduct [60]fullerenes have emerged as the notable success of 56π fullerenes (PCEs, 4.7−6.5%).[21−28] However, tris-, tetrakis-, or pentakis-adducts exhibited extremely low performance, due to the reduced short circuit current (J_{sc}) and/or fill factor (FF).[29−35] This results from a poor bulk heterojunction (BHJ) network and loose packing in the fullerene phase, indicative of

the general trade-off issue between J_{sc} (FF) and V_{oc} in fullerene-based OPVs.

An effective way to address this issue is a design of a multiadduct fullerene with a compact substituent. Matsuo et al. have developed 1,2-dihydromethano (CH$_2$) fullerene as the most sterically compact adduct.[36] Remarkably, hetero bis-adducts of CH$_2$/indene [60]fullerene [C$_{60}$(CH$_2$)(Ind)][37] and CH$_2$/o-quinodimethane (QM) [60]fullerene[37−39] achieved 5.7−5.9% PCE for P3HT-based OPVs. Moreover, CH$_2$/indene [70]fullerene[37] and tris-adduct of (CH$_2$)$_2$/QM [60]fullerene[39] boosted the PCEs to 6.4%, owing to the increased J_{sc} (11 mA cm^{-2}) and V_{oc} (0.95 V), respectively. Another approach to improve the electronic and packing nature of fullerene is an isolation of bis-adduct isomers by chromatography or tethering techniques.[40−45] Li et al. have investigated the effects of isomers of dihydronaphthyl-based [60]fullerene bis-adduct (NCBA) on device performance.[46] The highest PCE of 6.3% was found for the blend of P3HT and NCBA trans-3-isomer, because of the shallow LUMO level and high electron mobility arisen from its tight packing in the film state.

In this work, we report synthesis and characterization of hetero and homo bis-adduct [60]fullerenes based on a spiro-acetalized unit or its precursor (cyclohexanone) in combination with indene, PCBM, and CH_2 (Figure 1). 58π spiro-acetalized
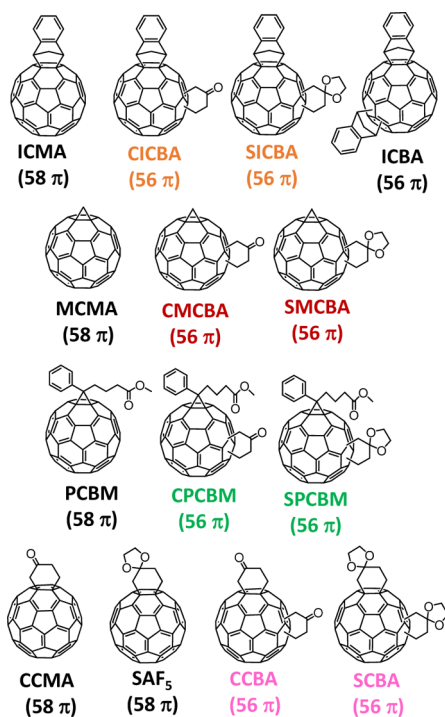

Figure 1. Chemical structures of hetero/homo bis-adduct and monoadduct fullerenes.

[60]fullerene monoadducts, SAF_n ($n = 5-7$, n denotes the size of the acetal ring)[47] is a central motif throughout this work. Previously, we have revealed that the solubility of SAF_n is controlled by the size of the acetal rings and consequent P3HT-based OPV outputs were enhanced from the five-membered ring SAF_5 (0.9%) to the seven-membered ring SAF_7 (4.0%), which were rationalized by the balance between space-charge-limited current (SCLC) hole and electron mobilities.[47] In addition, our studies[47,48] and literature[49] have shown that a good solubility is necessary for achieving a high PCE, while excessive solubility turns to suppress PCE, due to the decreased electron mobility. Having all that in mind, the least soluble SAF_5 among SAF_ns was chosen as the platform, because the presence of stereoisomers and the bulky unit of bis-adduct fullerene is expected to increase the solubility to a large extent. We performed a systematic investigation on the electrochemistry, solubility, morphology, and charge carrier mobility to consolidate the fundamental rule for designing hetero bis-adducts of fullerene for high-performing OPVs.

■ EXPERIMENTAL SECTION

Materials and Synthesis. Regioregular P3HT, fullerenes (C_{60}, PCBM, and ICBA), and solvents were purchased from Aldrich Inc., Frontier Carbon Inc., and Kishida Chemical Inc., respectively, and were used as received. Fullerene bis-adducts shown in Figure 1 were synthesized in a way similar to that of the previous report.[50] The details of the synthesis and compound data are provided in the Supporting Information. The structures of fullerene bis-adducts were determined by ^{1}H and ^{13}C NMR analysis and MALDI-TOF-MS spectroscopy. Reduction potentials E_1^{red} standardized by Fc/Fc$^+$ couple were evaluated by cyclic voltammetry using an Ag/AgCl

electrode and Pt as the working and counter electrodes in o-dichlorobenzene (DCB), respectively. The electrolytic solution of tetra-n-butylammonium hexafluorophosphate electrolytic in DCB (0.1 mol dm^{-3}) was prepared. Fullerene derivative was dissolved in electrolytic solution (10^{-4} mol dm^{-3}), and the solution was degassed by bubbling argon for at least 1 min. The LUMO levels were calculated from E_1^{red} using LUMO level = $-e$ (E_1^{red} + 4.8).[51]

Organic Photovoltaic Cell. P3HT and spiro-acetalized methano C_{60} bis-adduct (SMCBA) were dissolved in DCB at 1:0.6 wt % (1.0 wt % DCB, 13 mg mL^{-1} for P3HT and 7.8 mg mL^{-1} for SMCBA). P3HT and other fullerene derivatives were dissolved in DCB at the ratio of 1:1 (wt %; 1.5 wt % DCB, 19.5 mg mL^{-1} for each). An aqueous solution of PEDOT:PSS (Clevios P VP AI 4083) after passing through a 0.45 μm filter was spin-coated onto the cleaned ITIO/glass. The substrate was annealed on a hot plate at 120 °C for 10 min in the air followed by 180 °C annealing for 3 min in a nitrogen glovebox. The DCB solution was then cast on top of the PEDOT:PSS buffer layer in a glovebox by spin-coating at 1400 rpm for 15 s after passing through a 0.2 μm filter. The active layer with ca. 200 nm thickness was thermally annealed at 150 °C for 10 min. P3HT:SMCBA were spin-coated at 1200 rpm for 60 s to form a 100 nm thick active layer. No thermal annealing was performed for P3HT:SMCBA. A cathode consisting of 20 nm Ca and 100 nm Al layers was sequentially deposited through a shadow mask on top of the active layers by thermal evaporation in a vacuum chamber. The resulting device configuration was ITO (120−160 nm)/PEDOT:PSS (45−60 nm)/active layer (ca. 100−200 nm)/Ca (20 nm)/Al (100 nm) with an active area of 7.1 mm^2. Current−voltage ($J-V$) curves were measured using a source-measure unit (ADCMT Corp., 6241A) under AM 1.5 G solar illumination at 100 mW cm^{-2} (1 sun, monitored by a calibrated standard cell, Bunko Keiki SM-250 KD) from a 300 W solar simulator (SAN-EI Corp., XES-301S).[52,53] Atomic force microscopy (AFM) observations were performed by a Seiko Instruments Inc. model Nanocute OP and Nanonavi II.

Space-Charge-Limited Current. The device structures of SCLC were the ITO/PEDOT:PSS/active layer (ca. 90−200 nm)/Au for hole, and Al/Active layer (ca. 100−230 nm)/LiF/Al for electron, respectively. The other procedures are the same with the OPV device fabrication. The active layer (blend of P3HT and fullerene) was prepared under the optimized condition. The hole or electron mobility was determined by fitting the $J-V$ curve into Mott−Gurney law ($J = 9\varepsilon_r\varepsilon_0\mu V^2/(8d^3)$), where ε_0 is the permittivity of free space, ε_r is the relative dielectric constant of the material, μ is the hole (or electron) mobility, V is the voltage, and d is the layer thickness.[54−56]

■ RESULTS AND DISCUSSION

Synthesis. The hetero bis-adducts with cyclohexanone and five-membered acetalized ring were synthesized according to the slightly modified method of the reference[50] (upper panel of Scheme 1). The Diels−Alder reactions of representative 58π fullerene derivatives, 1,2-dihydromethano C_{60} monoadduct (MCMA),[36] indene C_{60} monoadduct (ICMA), and PCBM were carried out in DCB in the presence of excess 2-trimethylsilyloxy-1,3-butadiene (1.5−2.0 equiv) at reflux temperature for 1.5 h. The resulting [2 + 4] bis-adducts were readily decomposed on silica gel column chromatography to afford cyclohexanone-fused fullerene bis-adduct derivatives: cyclohexanone methano C_{60} bis-adduct (CMCBA), cyclohexanone indene C_{60} bis-adduct (CICBA), and cyclohexanone phenyl-C_{61}-butylic acid methyl ester (CPCBM), in moderate yields (36−70%). Subsequently, these cyclohexanone-fused fullerenes were reacted with 1,2-ethylenediol in the presence of TiCl$_4$ (ca. 20 equiv) in DCB/tetrahydrofuran (THF)/1,2-ethylenediol (5/5/1 (v/v/v)) at 40 °C for 16 h, which affords spiro-acetalized methano C_{60} bis-adduct (SMCBA), spiro-acetalized indene C_{60} bis-adduct (SICBA), and spiro-acetalized phenyl-C_{61}-butylic acid methyl ester (SPCBM) in good yields

Scheme 1. Synthesis of Fullerene Bis-Adducts[a]
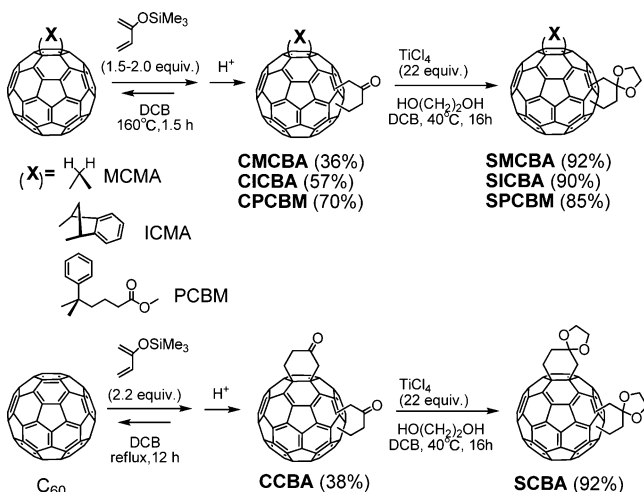
[a]The values in the brackets are the yield.

(85–92%). The homo bis-adducts of cyclohexanone C_{60} bis-adduct (CCBA) and spiro-acetalized C_{60} bis-adduct (SCBA) were also prepared according to the lower panel of Scheme 1.

After purification by silica gel column chromatography (CS_2/ethyl acetate eluent gradient system), the fullerene bis-adducts were characterized by ^1H NMR, ^{13}C NMR, MALDI-TOF-MS, and HPLC (Supporting Information Figures S1–S8). It should be mentioned that all products contain a mixture of regioisomers, because of the possible eight or nine positions of the secondary substituent for homo or hetero bis-adducts, respectively (Figure 2a).[57−59] Additionally, the regioisomers of
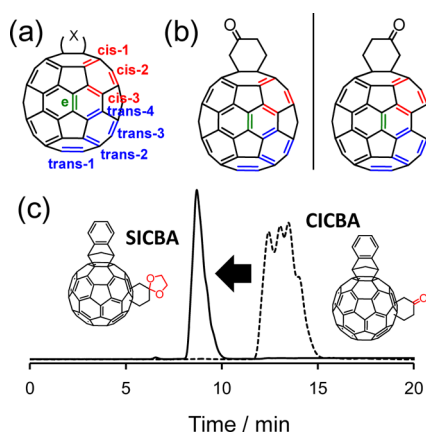

Figure 2. Eight possible regioisomers of a C_{60} bis-adduct substituted with (a) a symmetrical added and (b) an unsymmetrical added. (c) HPLC chromatograms detected by COSMOSIL Buckyprep column of CICBA (dotted line) and SICBA (solid line).

cyclohexanone-fused fullerenes are doubled, due to their unsymmetric structures (Figure 2b). For instance, at least six regioisomers exist in CICBA and SICBA, as dictated from the HPLC chromatograms (Figure 2c and Supporting Information Figure S9) and ^{13}C NMR spectra in the range of carbonyl group (δ = 210 ppm) and acetalized carbon (δ = 110 ppm) (Supporting Information Figures S5 and S6). Similarly, CCBA/SCBA/CMCBA/SMCBA and CPCBM/SPCBM have three and five regioisomers, respectively. These regioisomers allow good solubility suitable for OPV application. The thermogravi-

metric analysis (TGA) of monoadduct (SAF_5) has been performed previously, where its weight loss was not observed until 350 °C.[50] This excellent thermal stability comparable to PCBM[60] is due to the small strain energy of the five-membered spiro-acetalized ring.

Energy Level and Solubility. The photophysical properties of the bis- and mono-adduct C_{60} were evaluated by UV−vis photoabsorption spectroscopy. As shown in Supporting Information Figure S10, the bis-adducts in dilute toluene solutions (2×10^{-5} mol dm^{-3}) displayed a stronger and broader absorption than monoadducts in the visible region, by virtue of resolved degeneracy via symmetry break. The optical bandgaps of fullerenes estimated from the absorption edge indicated a reasonable increase by 0.12−0.15 eV in 56π hetero bis-adducts compared to their 58π mono-adduct precursors (Table 1 and Supporting Information Figure S11). Acetalization of cyclohexanone expanded the bandgap by 0.02−0.07 eV, due to the electron-donating ability of the spiro-acetalized unit.[47,48]

Table 1. Electrochemical Properties and Solubilities

compound	E_g/eV[a]	E^1_{red}/V[b]	LUMO/eV[c]	HOMO/eV[d]	solubility/ (wt %)[e]
C_{60}	1.84	−1.09	−3.71	−5.55	
CCMA[f]	1.85	−1.17	−3.71	−5.56	0.5
SAF$_5$[f]	1.90	−1.19	−3.61	−5.51	0.2
SCBA	2.17	−1.36	−3.44	−5.61	2.2
CCBA	2.15	−1.27	−3.53	−5.68	2.3
MCMA	1.90	−1.19	−3.61	−5.51	0.1
SMCBA	2.12	−1.32	−3.48	−5.61	0.7
CMCBA	2.05	−1.28	−3.52	−5.57	0.9
ICMA	1.87	−1.21	−3.59	−5.46	0.8
SICBA	2.14	−1.36	−3.44	−5.58	3.6
CICBA	2.10	−1.30	−3.50	−5.60	5.1
ICBA	2.15	−1.36	−3.44	−5.59	6.6
PCBM[f]	1.90	−1.19	−3.61	−5.51	1.0
SPCBM	2.14	−1.31	−3.49	−5.63	7.0
CPCBM	2.12	−1.27	−3.53	−5.65	10

[a]Optical bandgap energy evaluated from the absorption edge in DCB. [b]The first reduction wave in DCB relative to Fc/Fc$^+$. [c]LUMO levels evaluated by CV in DCB via LUMO = $-e(4.8 + E^1_{red})$. [d]HOMO was calculated by subtracting E_g from the LUMO. [e]In toluene. [f]Taken from ref 47.

A rise of LUMO levels is a pronounced advantage of fullerene bis-addition. The LUMOs were measured by cyclic voltammetry (CV) in DCB using an Ag/AgCl electrode and Pt as the working and counter electrodes, respectively (Table 1). All compounds exhibited two or three reversible one-electron-reduction waves, where the change of electric potential is reasonably explained by the reduction of the π-electron system and electron affinity of substituent (Supporting Information Table S1 and Figure S12). For instance, addition of a cyclohexanone group to ICMA (58π) raised the LUMO level by 0.1 eV, simply owing to the shrinkage of the fullerene π-system (56π). Acetalization of CICBA yielding SICBA further lifted the LUMO level by 0.05 eV due to the electron-donating nature of the spiro-acetalized moiety. A similar trend was observed for the CH_2 and PCBM series. The highest occupied molecular orbital (HOMO) energies were calculated by subtracting the optical bandgap from the LUMO in solutions. The LUMO and HOMO levels of the fullerenes are
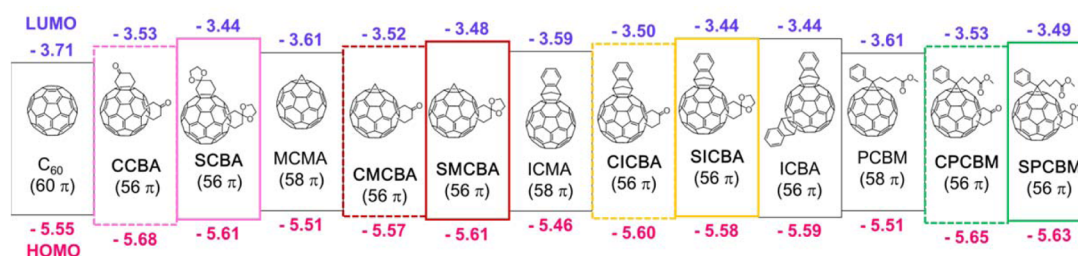
Figure 3. LUMO and HOMO energy levels of fullerenes, which were evaluated by CV in DCB and subtraction of E_g from the LUMO, respectively.
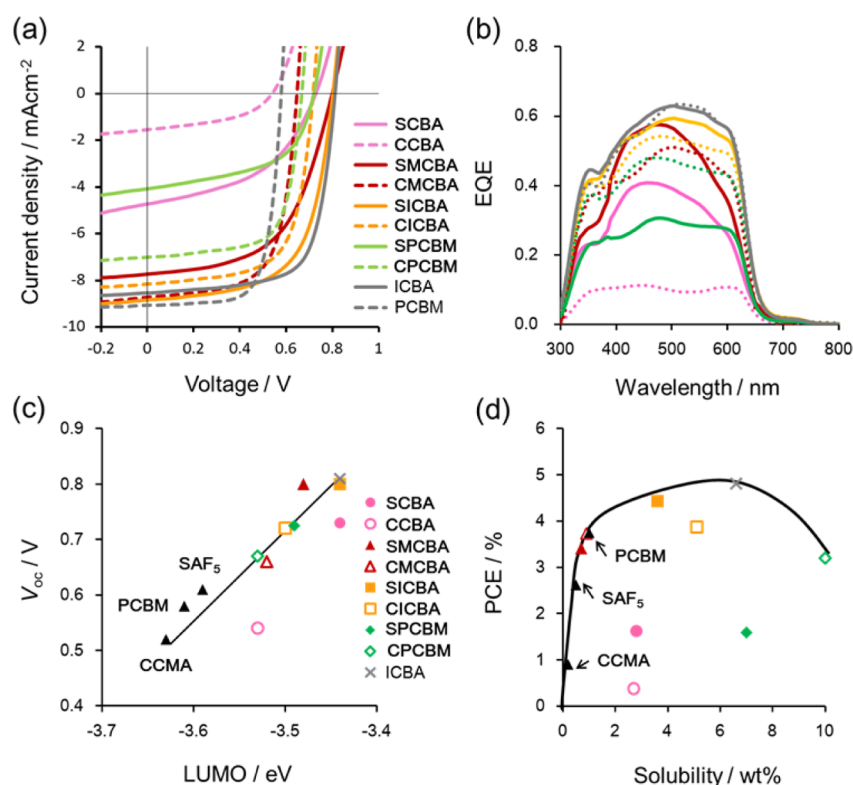

Figure 4. (a) $J-V$ curves for P3HT:fullerene (1:1 or 1:0.6 (w/w)) devices under AM 1.5G (100 mW cm^{-2}). (b) EQE spectra of the devices. (c) V_{oc} vs LUMO levels measured by CV in DCB. The solid line is an eye-guide. (d) PCE vs solubility of fullerene in toluene. The solid lines in c and d are eye-guides. The solid black triangles in c and d represent SAF$_S$, ketone, and PCBM, respectively, taken from ref 47.

Table 2. OPV Performances of P3HT:Fullerene Devices under AM 1.5G (100 mW cm^{-2})

entry	J_{sc} $(J_{sc\,av})$/ (mA cm^{-2})[d]	J_{sc}^{calc}/(mA cm^{-2}) (J_{sc}/J_{sc}^{calc})[e]	V_{oc} $(V_{oc\,av})$/V[d]	FF (FF$_{av}$)[d]	PCE (PCE$_{av}$)/%[d]	R_a (nm)[f]
CCMA[a,b]	7.55 (7.51)		0.52 (0.52)	0.67 (0.67)	2.62 (2.59 ± 0.03)	7.3
SAF$_S$[a,b]	3.55 (3.48)		0.61 (0.61)	0.42 (0.42)	0.90 (0.89 ± 0.01)	
SCBA[a]	4.73 (4.74)	5.09 (0.93)	0.73 (0.72)	0.47 (0.45)	1.62 (1.59 ± 0.03)	12.7
CCBA[a]	1.55 (1.53)	1.63 (0.95)	0.54 (0.53)	0.46 (0.44)	0.38 (0.36 ± 0.02)	14.9
SMCBA[c]	7.73 (7.44)	6.92 (1.12)	0.80 (0.80)	0.55 (0.50)	3.41 (3.20 ± 0.21)	5.5
CMCBA[a]	8.28 (8.58)	6.84 (1.21)	0.66 (0.65)	0.69 (0.66)	3.73 (3.69 ± 0.04)	8.9
SICBA[a]	8.84 (8.82)	8.36 (1.06)	0.80 (0.80)	0.63 (0.62)	4.43 (4.36 ± 0.07)	6.4
CICBA[a]	8.15 (8.12)	7.67 (1.06)	0.72 (0.72)	0.66 (0.66)	3.87 (3.82 ± 0.05)	7.6
SPCBM[a]	4.08 (4.00)	4.26 (0.96)	0.72 (0.72)	0.54 (0.54)	1.59 (1.56 ± 0.03)	5.4
CPCBM[a]	7.01 (6.99)	6.83 (1.03)	0.67 (0.67)	0.69 (0.69)	3.20 (3.19 ± 0.01)	4.9
ICBA[a]	8.54 (8.60)	8.77 (0.97)	0.81 (0.81)	0.69 (0.69)	4.81 (4.76 ± 0.05)	11.5
PCBM[a]	9.06 (8.97)	8.64 (1.05)	0.58 (0.58)	0.71 (0.70)	3.75 (3.72 ± 0.03)	5.6

[a]P3HT:fullerene = 1:1 (wt %) processed from DCB (ITO/PEDOT:PSS/active layer/Ca/Al). Annealed at 150 °C for 10 min. [b]Taken from ref 47. [c]P3HT:fullerene = 1:0.6 (wt %) processed from DCB. No post-thermal annealing. [d]The averaged values in the brackets were evaluated from at least three devices. [e]J_{sc}^{cal} is a calculated J_{sc} from EQE spectrum. [f]Surface roughness in a 2 × 2 μm^2 AFM topological image (Supporting Information Figure S14).

summarized in Figure 3. The HOMO levels of bis-adducts remained mostly unchanged in the range from −5.51 to −5.68 eV.

The solubilities in toluene showed a wide variation ranging from 0.7 to 10 wt %. The indene- and PCBM-based hetero bis-adducts possess the higher solubilities (3.6−10 wt %) than their mono-adducts (PCBM, 1.5 wt %; ICMA, 0.8 wt %). The solubilities of spiro-acetalized hetero bis-adducts are slightly less than the cyclohexanone hetero bis-adducts, probably because the five-membered acetal ring restricts the flipping motion between boat and chair conformations. The homo bis-adducts of CCBA and SCBA are quite soluble (2.3 and 2.2 wt %), while the hetero bis-adducts of CH_2 and cyclohexanone/spiro-acetal (CMCBA and SMCBA) showed the reduced solubilites of 0.9 and 0.7 wt %, respectively. They are even comparable to the monoadducts of PCBM (1.0 wt %) and ICMA (0.8 wt %), due to the low solubility of CH_2 mono-adduct (MCMA, 0.1 wt %). However, all of the hetero and homo bis-adducts have enough solubilities in DCB for OPV device fabrication,[47] and thus they could be relevant to a detailed investigation on the solubility-device performance relationship.

Photovoltaic Outputs and Fullerene Solubility. The OPV performances of P3HT:bis-adduct (1:1 (w/w) or 1:0.6 (w/w)) were evaluated in a normal cell structure, according to the previous protocol.[52,53] The active layers with 100−200 nm in thickness were prepared by spin-coating of DCB solutions, followed by solvent annealing in a covered Petri dish and thermal annealing at 150 °C for 10 min. Figure 4a shows the current density versus voltage (J−V) curves under AM 1.5G illumination at 100 mW cm^{-2} (Table 2). It should be emphasized that SICBA exhibited the high PCE of 4.43% (PCE_{av} = 4.36 ± 0.07%) with J_{sc} of 8.84 mA cm^{-2}, V_{oc} of 0.80 V, and FF of 0.60, which is a remarkable enhancement from the corresponding mono-adduct (P3HT:SAF$_5$, PCE = 0.9%).[47] The best PCE was, however, lower than the high-performing P3HT:ICBA reference (PCE_{max} = 4.81%; PCE_{av} = 4.76 ± 0.05%), ascribed to the reduced FF. CICBA, the cyclohexanone precursor of SICBA was ranked at the second highest PCE of 3.87% (PCE_{av} = 3.82 ± 0.05%), where the reduced V_{oc} (0.72 V) is mainly responsible for the lower PCE of CICBA. The V_{oc} reduction from spiro-acetalized to cyclohexanone was generally observed in other hetero/homo bis-adducts and consistent with the deeper LUMO levels of the latter. The external quantum efficiency (EQE) spectra were almost similar except for the low-performing SPCBM, SCBA, and CCBA (Figure 4b), corresponding to their low J_{sc}s found in the J−V curves of Figure 4a. The calculated J_{sc} (=J_{sc}^{calc}) from the relevant EQE spectra are mostly in good agreement with the J_{sc}s under 1 sun within ±7% (Table 2). The relatively large difference found for SMCBA and CMCBA (12 and 21% lower J_{sc}^{calc} than J_{sc}, respectively) is probably caused by the degradation of the device after the JV curve measurements under 1 sun.

Figure 4c plots the V_{oc} as a function of LUMO level estimated by CV in DCB. The excellent linearity agrees with the LUMO dependence of fullerene on V_{oc}[61] and with the well-established relationship between V_{oc} and difference of HOMO of donor and LUMO of acceptor. As previously mentioned, V_{oc} generally increased from cyclohexanone to the spiro-acetalized unit for all of the hetero bis-adducts, reflecting the electron-donating nature of the latter. The homo bis-adducts of SCBA and CCBA showed ca. 0.1 V lower V_{oc} than the straight line, due to the low J_{sc}.

In a sharp contrast, PCE showed an asymmetric convex curve against the solubility of fullerene (Figure 4d) with the maximum at ca. 6.6 wt % (ICBA). Such a parabolic curve has been reported in other fullerene derivatives,[48,49,62,63] clearly demonstrating that excessive solubility degrades a PCE. Atomic force microscopy (AFM) images shown in Figure 5 (phase)
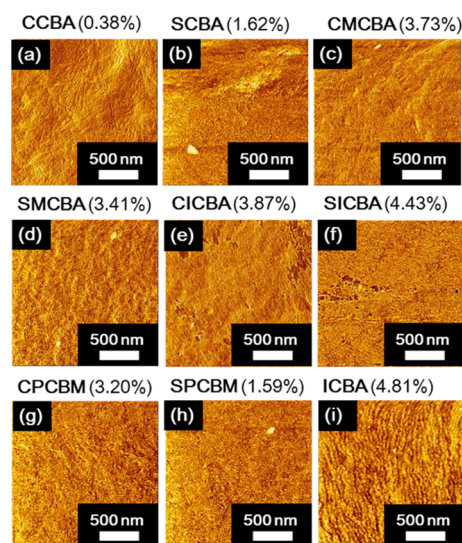

Figure 5. AFM phase images of P3HT:fullerene films at the OPV optimal condition. Images are observed for P3HT films blended with (a) CCBA, (b) SCBA, (c) CMCBA, (d) SMCBA, (e) CICBA, (f) SICBA, (g) CPCBM, (h) SPCBM, and (i) ICBA, respectively. The values in the brackets are the best PCE (Table 2). The image size is 2 × 2 μm^2.

and Supporting Information Figure S14 (topography) indicate no significant phase separation between polymer and fullerene, while CCBA and SCBA have a larger surface roughness (R_a, 12−15 nm) than the other bis-adducts (5−9 nm, Table 2). In fact, these two homo bis-adducts have a tendency of rather aggregation, resulting in the decrease of device performance. The insignificant change in morphology except for these homo bis-adducts suggests that the OPV performances are dominated by electronic factors rather than morphology.

Mobility Balance. In order to elucidate how the bis-adduct structures and their electronic features affect the OPV performances, charge carrier mobilities of the blend films were investigated by SCLC technique (Supporting Information Figure S13).[54−56] Table 3 lists the hole mobility (μ_h), electron mobility (μ_e), and their ratio (μ_e/μ_h). Charge carrier mobilities exhibited a large variation by the orders of magnitude from 10^{-7} to 10^{-3} cm^2 V^{-1} s^{-1} for holes (Figure 6a) and 10^{-8} to 10^{-3} cm^2 V^{-1} s^{-1} for electrons (Figure 6b). The PCE vs μ_h or μ_e displays mostly scattered plots; however, a strong positive correlation was deciphered for the PCE vs μ_e/μ_h ranging from 10^{-3} to 10^{-1} (Figure 6c). This highlights the superiority of mobility balance in the devices' performance, in good accordance with the simulation reported by Kotlarski and Blom[64] and experiments of our previous monoadduct fullerenes.[47,48] Surprisingly, the correlation of mobility balance vs PCE can be interpolated among not only the high-performing bis-adducts but also the monoadducts of SAF$_5$, CCMA, and PCBM, although the PCEs contain the large difference of V_{oc} (ca. 0.5−0.8 V). This correlation is observable in multiaddduct fullerenes,[31] the thermal annealing process of P3HT:PCBM,[65] and its p/n

Table 3. SCLC Hole and Electron Mobilities and Their Balance in P3HT:Fullerene

acceptor	$\mu_h/(cm^2\ V^{-1}\ s^{-1})$	$\mu_e/(cm^2\ V^{-1}s^{-1})$	μ_e/μ_h
CCMA	2.2×10^{-4}	4.6×10^{-7}	2.1×10^{-3}
SAF$_5$,[a]	1.1×10^{-4}	1.5×10^{-9}	1.4×10^{-5}
SCBA	4.5×10^{-3}	3.0×10^{-4}	6.7×10^{-2}
CCBA	6.9×10^{-3}	6.7×10^{-6}	9.7×10^{-4}
SMCBA	5.2×10^{-7}	3.4×10^{-8}	6.5×10^{-2}
CMCBA	1.4×10^{-3}	5.4×10^{-5}	3.9×10^{-2}
SICBA	2.8×10^{-3}	1.2×10^{-3}	0.40
CICBA	1.2×10^{-3}	5.7×10^{-5}	4.8×10^{-2}
SPCBM	2.8×10^{-3}	3.4×10^{-5}	1.2×10^{-2}
CPCBM	2.0×10^{-3}	1.9×10^{-4}	9.5×10^{-2}
ICBA	4.9×10^{-3}	1.1×10^{-3}	2.2
PCBM	5.5×10^{-4}	1.5×10^{-3}	2.7

[a]Taken from ref 47.

composition.[66] SMCBA, of which active layer thickness was ca. 100 nm (others are ca. 200 nm) and the p/n ratio was 1:0.6 (others are 1:1), displayed exceptionally low μ_h and μ_e on the order of 10^{-8}–10^{-7} cm^2 V^{-1} s^{-1}. Nonetheless, the μ_e/μ_h (6.5 × 10^{-2}) and PCE (3.4%) of SMCBA lies on the general PCE trend found for the other fullerenes. This reiterates that the mobility balance rather than the absolute value of mobility is a key factor of solar cell performance. It should be noted that a thin active layer is necessary to maximize PCE in the case of low charge carrier mobilities such as for SMCBA. When a P3HT:SMCBA device was fabricated with 200 nm thickness and 1:1 p/n blend ratio, the PCE was considerably decreased to ca. 0.5%. The similar results have been reported for other multiadduct fullerenes (ca. 100 nm thickness and 1:0.6 p/n blend ratio),[27,30,38,39,45] although the underlying cause is complicated (interplay of mobility, lifetime, thickness, and BHJ structure) and not unraveled.

On the other hand, we need to mention that the low-performing bis-adducts of SPCBM (PCE$_{max}$ = 1.59%), SCBA (PCE$_{max}$ = 1.62%), and CCBA (PCE$_{max}$ = 0.38%) are far below the general line. Indeed, these three bis-adducts are also the exceptional group in the PCE plot with solubility shown in Figure 4d. They have moderate solubilities, high hole mobilities, and moderate electron mobilities, and thus the PCEs should be at least doubled. The reason for the low PCEs of these three bis-adducts is elusive. The presence of unknown impurity might impair the OPV outputs, because SPCBM and CCBA show slightly lower HPLC purities (97% and 98%) than the others (99–99.5%) (Supporting Information Figure S9).

Guide for Efficient Hetero Bis-Adduct Fullerene. Through the comprehensive characterization of hetero/homo bis-adducts of [60]fullerene, we identified the solubility as the rough indicator of PCE and mobility balance as the more precise factor (note that there are a few exceptions). The charge carrier mobilities are the results of device outputs after careful optimization of processing conditions including thickness, p/n blend, and solvent. However, solubility is a fundamental property which can be evaluated without device engineering. Therefore, a simple method to predict the solubility of hetero bis-adduct fullerene from the corresponding mono-adducts is useful for designing novel fullerene acceptors.
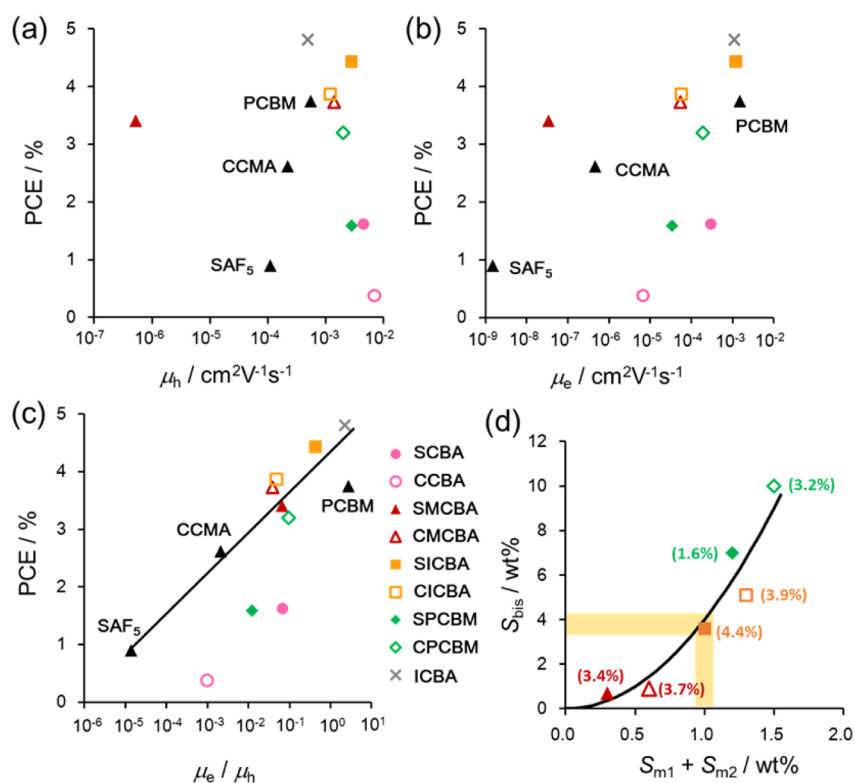

Figure 6. PCE vs logarithmic plots of SCLC (a) hole mobility (μ_h), (b) electron mobility (μ_e), and (c) their balance (μ_e/μ_h). The device parameters of SAF$_5$ were taken from ref 47. The solid line is an eye-guide. (d) Plot of experimental solubility of hetero bis-adduct [60]fullerenes in toluene, S_{bis}, vs the sums of solubilities of relevant monoadducts in toluene, S_{m1} and S_{m2}. The solid line is eq 1 (see text). The values in the brackets are the maximum PCE (Table 2). The correspondence of the colorized symbols in a–d is shown in the inset of c. The black triangles in a–c are mono-adduct fullerenes.

Figure 6d shows the experimentally evaluated solubilities of hetero bis-adduct [60]fullerenes, S_{bis} (wt % in toluene) as a function of the sum of solubilities of respective monoadduct [60]fullerenes, S_{m1} and S_{m2}. For example, the x-axis value (1.0 wt %) of SICBA (S_{bis} = 3.6 wt %) was calculated by adding ICMA (S_{m1} = 0.8 wt %, Table 1) and SAF$_5$ (S_{m2} = 0.2 wt %).[47] Interestingly, S_{bis} seems to increase superlinearly with $S_{m1} + S_{m2}$, indicative of the cooperative enhancement via two solubilizing substituents and the presence of regioisomers. On the basis of the six hetero bis-adducts evaluated in this study, the following empirical equation was deduced.

$$S_{bis} = a(S_{m1} + S_{m2})^2 \quad (1)$$

where a is the prefactor approximated to be 4 (wt %)$^{-1}$. We note that the validity of this equation is limited in S_{bis} < 10 wt %. In the present study, the solubilities of hetero bis-adducts (S_{bis}) giving the first and second highest PCEs of SICBA and CICBA were 3.6 and 5.1 wt %, respectively. The PCEs of P3HT-based OPVs blended with $C_{60}(CH_2)(Ind)$ and $C_{60}(CH_2)(QM)$ were 5.9 and 5.0%, where their solubilities were 4.0 wt % in toluene.[37] Thus, the most optimal solubility of hetero bis-adduct is expected around 4 wt % drawn by the yellow area in Figure 6d, which corresponds to $S_{m1} + S_{m2}$ = 1 wt % (=8.7 mg mL^{-1} in toluene). Interestingly, this solubility is close to that of PCBM (1.0 wt % in toluene) which is the most compatible fullerene with a wide range of p-type semiconductors. Note that the PCBM solubility in chlorobenzene (4.3 wt %, 50 mg mL^{-1}) is much higher than that in toluene.[67]

It should be mentioned that the solubility is not the sole determinant but other complicated factors such as interaction and miscibility with polymer, driving force for formation of fullerene pure domain, and film processability markedly influence the device performances. Troshin et al. have clarified the unusual double branched dependence of PCE on the fullerene solubility, which also depends on the counter polymer and solvent to a large extent.[67] However, the empirical relationship can serve as one of the design guides for the development of efficient OPV fullerenes, because the molecular design of hetero bis-adduct has a myriad of combinations.

CONCLUSION

We performed a systematic study on the [60]fullerene homo bis-adducts of cyclohexanone or five-membered spiro-acetalized ring (SAF$_5$) and their hetero bis-adducts with CH$_2$, indene, and PCBM. These 56π bis-adducts rationally gave advantages in both solubility and LUMO level. The best PCE of 4.43% (PCE$_{av}$ = 4.36 ± 0.07%) was obtained for P3HT:SICBA, mainly due to the high V_{oc} (0.80 V). The OPV device performances were found to correlate roughly with the solubility and more precisely with the SCLC mobility balance of holes and electrons, although there were a few exceptions associated with elusive factors (e.g., impurity and anomalous change of film quality). Based on the characterization of solubility and P3HT-based OPV device, we proposed the empirical equation to estimate the optimal solubility for hetero bis-adduct [60]fullerenes on the basis of the total solubility of respective monoadduct. It would be helpful for a coarse screening and designing of bis-adduct fullerenes for efficient OPV.

ASSOCIATED CONTENT

⑤ Supporting Information

Text describing the experimental materials and synthesis and the compound data, Table S1 listing reduction potentials of fullerene bis-adducts in DCB, and Figures S1−S8 showing ^{1}H and ^{13}C NMR results, Figure S9 showing HPLC results, Figures S10 and S11 showing UV−vis results, Figure S12 showing CVs, Figure S13 showing SCLC J−V curves, and Figure S14 showing AFM topography. The Supporting Information is available free of charge on the ACS Publications website at DOI: 10.1021/acsami.5b02456.

AUTHOR INFORMATION

Corresponding Authors
*(A.S.) E-mail: saeki@chem.eng.osaka-u.ac.jp.
*(K.K.) E-mail: kokubo@chem.eng.osaka-u.ac.jp.
*(S.S.) E-mail: seki@chem.eng.osaka-u.ac.jp.

Present Addresses
†Department of Molecular Engineering, Graduate School of Engineering, Kyoto University, A4-009 Kyoto University Katsura Campus, Nishikyo-ku, Kyoto 615-8510, Japan. E-mail: seki@moleng.kyoto-u.ac.jp.
‡Department of Chemistry, Massachusetts Institute of Technology, 77 Massachusetts Ave., Cambridge, MA 02139, United States.

Notes
The authors declare no competing financial interest.

REFERENCES

(1) Arias, A. C.; Mackenzie, J. D.; McCulloch, I.; Rivnary, J.; Salleo, A. Materials and Applications for Large Area Electronics: Solution-Based Approaches. *Chem. Rev.* **2010**, *110*, 3−24.
(2) Beaujuge, P. M.; Fréchet, J. M. Molecular Design and Ordering Effects in π-Functional Materials for Transistor and Solar Cell Applications. *J. Am. Chem. Soc.* **2011**, *133*, 20009−20029.
(3) Janssen, R. A. J.; Nelson, J. Factors Limiting Device Efficiency in Organic Photovoltaics. *Adv. Mater.* **2013**, *25*, 1847−1858.
(4) Li, G.; Shrotriya, V.; Huang, J.; Yao, Y.; Moriarty, T.; Emery, K.; Yang, Y. High-Efficiency Solution Processable Polymer Photovoltaic Cells by Self-Oorganization of Polymer Blends. *Nat. Mater.* **2005**, *4*, 864−868.
(5) Kim, Y.; Cook, S.; Tuladhar, S. M.; Choulis, S. A.; Nelson, J.; Durrant, J. R.; Bradley, D. C.; Giles, M.; McCulloch, I.; Ha, C. S.; Ree, M. A Strong Regioregularity Effect in Self-Organizing Conjugated Polymer Films and High-Efficiency Polythiophene:Fullerene Solar Cells. *Nat. Mater.* **2006**, *5*, 197−203.
(6) Dang, M. T.; Hirsch, L.; Wantz, G. P3HT:PCBM, Best Seller in Polymer Photovoltaic Research. *Adv. Mater.* **2011**, *23*, 3597−3602.
(7) Heeger, A. J. 25th Anniversary Article: Bulk Heterojunction Solar Cells: Understanding the Mechanism of Operation. *Adv. Mater.* **2014**, *26*, 10−28.
(8) Szarko, J. M.; Rolczynski, B. S.; Lou, S. J.; Xu, T.; Strzalka, J.; Marks, T. J.; Yu, L.; Chen, L. X. Photovoltaic Function and Exciton/Charge Transfer Dynamics in a Highly Efficient Semiconducting Copolymer. *Adv. Funct. Mater.* **2014**, *24*, 10−26.
(9) Lei, T.; Wang, J.-Y.; Pei, J. Roles of Flexible Chains in Organic Semiconducting Materials. *Chem. Mater.* **2014**, *26*, 594−603.

(10) Dimitrov, S. D.; Durrant, J. R. Materials Design Considerations for Charge Generation in Organic Solar Cells. *Chem. Mater.* **2014**, *26*, 616−630.

(11) Guo, X.; Zhou, N.; Lou, S. J.; Smith, J.; Tice, D. B.; Hennek, J. W.; Ortiz, R. P.; Navarrete, J. T. L.; Li, S.; Strzalka, J.; Chen, L. X.; Chang, R. P. H.; Facchetti, A.; Marks, T. J. Polymer Solar Cells with Enhanced Fill Factors. *Nat. Photonics* **2013**, *7*, 825−833.

(12) Nguyen, T. L.; Choi, H.; Ko, S.-J.; Uddin, M. A.; Walker, B.; Yum, S.; Jeong, J.-E.; Yun, M. H.; Shin, T. J.; Hwang, S.; Kim, J. Y.; Woo, H. Y. Semi-Crystalline Photovoltaic Polymers with Efficiency Exceeding 9% in a ~300 nm Thick Conventional Single-Cell Device. *Energy Environ. Sci.* **2014**, *7*, 3040−3051.

(13) Kong, J.; Hwang, I.-W.; Lee, K. Top-Down Approach for Nanophase Reconstruction in Bulk Heterojunction Solar Cells. *Adv. Mater.* **2014**, *26*, 6275−6283.

(14) Ye, L.; Zhang, S.; Zhao, W.; Yao, H.; Hou, J. Highly Efficient 2D-Conjugated Benzodithiophene-Based Photovoltaic Polymer with Linear Alkylthio Side Chain. *Chem. Mater.* **2014**, *26*, 3603−3605.

(15) Liu, Y.; Zhao, J.; Li, Z.; Mu, C.; Ma, W.; Hu, H.; Jiang, K.; Lin, H.; Ade, H.; Yan, H. Aggregation and Morphology Control Enables Multiple Cases of High-Efficiency Polymer Solar Cells. *Nat. Commun.* **2014**, *5*, 5293/1−5293/8.

(16) Li, K.; Li, Z.; Feng, K.; Xu, X.; Wang, L.; Peng, Q. Development of Large Band-Gap Conjugated Copolymers for Efficient Regular Single and Tandem Organic Solar Cells. *J. Am. Chem. Soc.* **2013**, *135*, 13549−13557.

(17) Li, W.; Furlan, A.; Hendriks, K. H.; Wienk, M. M.; Janssen, R. A. Efficient Tandem and Triple-Junction Polymer Solar Cells. *J. Am. Chem. Soc.* **2013**, *135*, 5529−5532.

(18) You, J.; Dou, L.; Yoshimura, K.; Kato, T.; Ohya, K.; Moriarty, T.; Emery, K.; Chen, C. C.; Gao, J.; Li, G.; Yang, Y. A Polymer Tandem Solar Cell with 10.6% Power Conversion Efficiency. *Nat. Commun.* **2013**, *4*, 1446/1−1446/10.

(19) Scharber, M. C.; Mühlbacher, D.; Koppe, M.; Denk, P.; Waldauf, C.; Heeger, A. J.; Brabec, C. J. Design Rules for Donors in Bulk-Heterojunction Solar Cells—Towards 10% Energy-Conversion Efficiency. *Adv. Mater.* **2006**, *18*, 789−794.

(20) Lenes, M.; Wetzelaer, G.-J. A. H.; Kooistra, F. B.; Veenstra, S. C.; Hummelen, J. C.; Blom, P. W. M. Fullerene Bisadducts for Enhanced Open-Circuit Voltages and Efficiencies in Polymer Solar Cells. *Adv. Mater.* **2008**, *20*, 2116−2119.

(21) He, Y.; Chen, H.-Y.; Hou, J.; Li, Y. Indene-C_{60} Bisadduct: A New Acceptor for High-Performance Polymer Solar Cells. *J. Am. Chem. Soc.* **2010**, *132*, 1377−1382.

(22) Zhao, G.; He, Y.; Li, Y. 6.5% Efficiency of Polymer Solar Cells Based on Poly(3-hexylthiophene) and Indene-C_{60} Bisadduct by Device Optimization. *Adv. Mater.* **2010**, *22*, 4355−4358.

(23) Guo, X.; Zhang, M.; Cui, C.; Hou, J.; Li, Y. Efficient Polymer Solar Cells Based on Poly(3-hexylthiophene) and Indene-C_{60} Bisadduct Fabricated with Non-Halogenated Solvents. *ACS Appl. Mater. Interfaces* **2014**, *6*, 8190−8198.

(24) Miller, N. C.; Sweetnam, S.; Hoke, E. T.; Gysel, R.; Miller, C. E.; Bartelt, J. A.; Xie, X.; Toney, M. F.; McGehee, M. D. Molecular Packing and Solar Cell Performance in Blends of Polymers with a Bisadduct Fullerene. *Nano Lett.* **2012**, *12*, 1566−1570.

(25) Cheng, Y.-J.; Liao, M.-H.; Chang, C.-Y.; Kao, W.-S.; Wu, C.-E.; Hsu, C.-S. Di(4-methylphenyl)methano-C_{60} Bis-Adduct for Efficient and Stable Organic Photovoltaics with Enhanced Open-Circuit Voltage. *Chem. Mater.* **2011**, *23*, 4056−4062.

(26) He, Y.; Peng, B.; Zhao, G.; Zou, Y.; Li, Y. Indene Addition of [6,6]Phenyl-C_{61}-butyric Acid Methyl Ester for High-Performance Acceptor in Polymer Solar Cells. *J. Phys. Chem. C* **2011**, *115*, 4340−4344.

(27) Zhang, C.; Chen, S.; Xiao, Z.; Zuo, Q.; Ding, L. Synthesis of Mono- and Bisadducts of Thieno-*o*-quinodimethane with C_{60} for Efficient Polymer Solar Cells. *Org. Lett.* **2012**, *16*, 1508−1511.

(28) Li, Y. Fullerene-Bisadduct Acceptors for Polymer Solar Cells. *Chem.—Asian J.* **2013**, *8*, 2316−2328.

(29) Lenes, M.; Shelton, S. W.; Sieval, A. B.; Kronholm, D. F.; Hummelen, J. C.; Blom, P. W. M. Electron Trapping in Higher Adduct Fullerene-Based Solar Cells. *Adv. Funct. Mater.* **2009**, *19*, 3002−3007.

(30) Kim, K.-H.; Kang, H.; Nam, S. Y.; Jung, J.; Kim, P. S.; Cho, C.-H.; Lee, C.; Yoon, S. C.; Kim, B. J. Facile Synthesis of *o*-Xylenyl Fullerene Multiadducts for High Open Circuit Voltage and Efficient Polymer Solar Cells. *Chem. Mater.* **2011**, *23*, 5090−5095.

(31) Kang, H.; Cho, C.-H.; Cho, H.-H.; Kang, T. E.; Kim, H. J.; Kim, K.-H.; Yoon, S. C.; Kim, B. J. Controlling Number of Indene Solubilizing Groups in Multiadduct Fullerenes for Tuning Optoelectronic Properties and Open-Circuit Voltage in Organic Solar Cells. *ACS Appl. Mater. Interfaces* **2012**, *4*, 110−116.

(32) Liu, C.; Xu, L.; Chi, D.; Li, Y.; Liu, H.; Wang, J. Synthesis of Novel Acceptor Molecules of Mono- and Multiadduct Fullerene Derivatives for Improving Photovoltaic Performance. *ACS Appl. Mater. Interfaces* **2013**, *5*, 1061−1069.

(33) Kennedy, R. D.; Ayzner, A. L.; Wanger, D. D.; Day, C. T.; Halim, M.; Khan, S. I.; Tolbert, S. H.; Schwartz, B. J.; Rubin, Y. Self-Assembling Fullerenes for Improved Bulk-Heterojunction Photovoltaic Devices. *J. Am. Chem. Soc.* **2008**, *130*, 17290−17292.

(34) Niinomi, T.; Matsuo, Y.; Hashiguchi, M.; Sato, Y.; Nakamura, E. Penta(organo)[60]Fullerenes as Acceptors for Organic Photovoltaic Cells. *J. Mater. Chem.* **2009**, *19*, 5804−5811.

(35) Mikie, T.; Saeki, A.; Ikuma, N.; Kokubo, K.; Seki, S. Exploring Photovoltaic Feasibility of Pentaaryl [60]Fullerene in Bulk Heterojunction Architecture. *J. Photopolym. Sci. Technol.* **2014**, *27*, 553−556.

(36) Zhang, Y.; Matsuo, Y.; Li, C.-Z.; Tanaka, H.; Nakamura, E. A Scalable Synthesis of Methano[60]fullerene and Congeners by the Oxidative Cyclopropanation Reaction of Silylmethylfullerene. *J. Am. Chem. Soc.* **2011**, *133*, 8086−8089.

(37) Matsuo, Y.; Kawai, J.; Inada, H.; Nakagawa, T.; Ota, H.; Otsubo, S.; Nakamura, E. Addition of Dihydromethano Group to Fullerenes to Improve the Performance of Bulk Heterojunction Organic Solar Cells. *Adv. Mater.* **2013**, *25*, 6266−6269.

(38) Ye, G.; Chen, S.; Xiao, Z.; Wei, Q.; Ding, L. *o*-Quinodimethane-Methano[60]Fullerene and Thieno-*o*-Quinodimethane-Methano[60]-Fullerene as Efficient Acceptor Materials for Polymer Solar Cells. *J. Mater. Chem.* **2012**, *22*, 22374−22377.

(39) He, D.; Du, X.; Xiao, Z.; Ding, L. Methanofullerenes, $C_{60}(CH_2)_n$ (n = 1, 2, 3), as Building Blocks for High-Performance Acceptors Used in Organic Solar Cells. *Org. Lett.* **2014**, *16*, 612−615.

(40) Kitaura, S.; Kurotobi, K.; Sato, M.; Takano, Y.; Umeyama, T.; Imahori, H. Effects of Dihydronaphthyl-Based [60]Fullerene Bisadduct Regioisomers on Polymer Solar Cell Performance. *Chem. Commun. (Cambridge, U. K.)* **2012**, *48*, 8550−8552.

(41) Tao, R.; Umeyama, T.; Kurotobi, K.; Imahori, H. Effects of Alkyl Chain Length and Substituent Pattern of Fullerene Bis-Adducts on Film Structures and Photovoltaic Properties of Bulk Heterojunction Solar Cells. *ACS Appl. Mater. Interfaces* **2014**, *6*, 17313−17322.

(42) Sabirov, D. S. Anisotropy of Polarizability of Fullerene Higher Adducts for Assessing the Efficiency of Their Use in Organic Solar Cells. *J. Phys. Chem. C* **2013**, *117*, 9148−9153.

(43) Liao, M.-H.; Lai, Y.-Y.; Lai, Y.-Y.; Chen, Y.-T.; Tsai, C.-E.; Liang, W.-W.; Cheng, Y.-J. Reducing Regioisomers of Fullerene-Bisadducts by Tether-Directed Remote Functionalization: Investigation of Electronically and Sterically Isomeric Effects on Bulk-Heterojunction Solar Cells. *ACS Appl. Mater. Interfaces* **2014**, *6*, 996−1004.

(44) Umeyama, T.; Imahori, H. Design and Control of Organic Semiconductors and Their Nanostructures for Polymer-Fullerene-Based Photovoltaic Devices. *J. Mater. Chem. A* **2014**, *2*, 11545−11560.

(45) Tao, R.; Umeyama, T.; Higashino, T.; Koganezawa, T.; Imahori, H. A Single Cis-2 Regioisomer of Ethylene-Tethered Indene Dimer-Fullerene Adduct as an Electron-Acceptor in Polymer Solar Cells. *Chem. Commun. (Cambridge, U. K.)* **2015**, *51*, 8233−8236.

(46) Meng, X.; Zhao, G.; Xu, Q.; Tan, Z.; Zhang, Z.; Jiang, L.; Shu, C.; Wang, C.; Li, Y. Effects of Fullerene Bisadduct Regioisomers on Photovoltaic Performance. *Adv. Funct. Mater.* **2014**, *24*, 158−163.

(47) Mikie, T.; Saeki, A.; Masuda, H.; Ikuma, N.; Kokubo, K.; Seki, S. New Efficient (Thio)Acetalized Fullerene Monoadducts for Organic Solar Cells: Characterization Based on Solubility, Mobility Balance, and Dark Current. *J. Mater. Chem. A* **2015**, *3*, 1152−1157.

(48) Mikie, T.; Saeki, A.; Ikuma, N.; Kokubo, K.; Seki, S. Spiro-1, 3-Dioxolanofullerenes with Low-Lying LUMO Level for Organic Solar Cells. *Chem. Lett.* **2015**, *44*, 282−284.

(49) Troshin, P. A.; Hoppe, H.; Renz, J.; Egginger, M.; Mayorova, J. Y.; Goryachev, A. E.; Peregudov, A. S.; Lyubovskaya, R. N.; Gobsch, G.; Sariciftci, N. S.; Razumov, V. F. Material Solubility-Photovoltaic Performance Relationship in the Design of Novel Fullerene Derivatives for Bulk Heterojunction Solar Cells. *Adv. Funct. Mater.* **2009**, *19*, 779−788.

(50) Kokubo, K.; Masuda, H.; Ikuma, N.; Mikie, T.; Oshima, T. Synthesis and Characterization of New Acetalized [60]Fullerenes. *Tetrahedron Lett.* **2013**, *54*, 3510−3513.

(51) Liu, M. S.; Jiang, X.; Liu, S.; Herguth, P.; Jen, A. K.-Y. Effect of Cyano Substituents on Electron Affinity and Electron-Transporting Properties of Conjugated Polymers. *Macromolecules* **2002**, *35*, 3532−3538.

(52) Saeki, A.; Tsuji, M.; Seki, S. Direct Evaluation of Intrinsic Optoelectronic Performance of Organic Photovoltaic Cells with Minimizing Impurity and Degradation Effects. *Adv. Energy Mater.* **2011**, *1*, 661−669.

(53) Saeki, A.; Tsuji, M.; Yoshikawa, S.; Gopal, A.; Seki, S. Boosting Photovoltaic Performance of a Benzobisthiazole Based Copolymer: A Device Approach Using a Zinc Oxide Electron Transport Layer. *J. Mater. Chem. A* **2014**, *2*, 6075−6080.

(54) Blom, P. W. M.; de Jong, M. J. M.; Vleggaar, J. J. M. Electron and Hole Transport in Poly(p-phenylene vinylene) Devices. *Appl. Phys. Lett.* **1996**, *68*, 3308−3310.

(55) Melzer, C.; Koop, E. J.; Mihailetchi, V. D.; Blom, P. W. M. Hole Transport in Poly(phenylenevinylene)Methanofullerene Bulk-Heterojunction Solar Cells. *Adv. Funct. Mater.* **2004**, *14*, 865−870.

(56) Dunlap, D. H.; Parris, P. E.; Kenkre, V. M. Charge-Dipole Model for the Universal Field Dependence of Mobilities in Molecularly Doped Polymers. *Phys. Rev. Lett.* **1996**, *77*, 542−545.

(57) Nierengarten, J.-F.; Gramlich, V.; Cardullo, F.; Diederich, F. Regio- and Diastereoselective Bisfunctionalization of C_{60} and Enantioselective Synthesis of a C_{60} Derivative with a Chiral Addition Pattern. *Angew. Chem., Int. Ed.* **1996**, *35*, 2101−2013.

(58) Djojo, F.; Herzog, A.; Lamparth, I.; Hampel, F.; Hirsch, A. Regiochemistry of Twofold Additions to [6,6] Bonds in C_{60}: Influence of the Addend-Independent Cage Distortion in 1,2-Monoadducts. *Chem.—Eur. J.* **1996**, *2*, 1537−1547.

(59) Kordatos, K.; Bosi, S.; Ros, T. D.; Zambon, A.; Lucchini, V.; Prato, M. Isolation and Characterization of All Eight Bisadducts of Fulleropyrrolidine Derivatives. *J. Org. Chem.* **2001**, *66*, 2802−2808.

(60) Larson, B. W.; Whitaker, J. B.; Popov, A. A.; Kopidakis, N.; Rumbles, G.; Boltalina, O. V.; Strauss, S. H. Thermal [6,6] → [6,6] Isomerization and Decomposition of PCBM (Phenyl-C_{61}-butyric Acid Methyl Ester). *Chem. Mater.* **2014**, *26*, 2361−2367.

(61) Kooistra, F. B.; Knol, J.; Kastenberg, F.; Popescu, L. M.; Verhees, W. J. H.; Kroon, J. M.; Hummelen, J. C. Increasing the Open Circuit Voltage of Bulk-Heterojunction Solar Cells by Raising the LUMO Level of the Acceptor. *Org. Lett.* **2007**, *9*, 551−554.

(62) Renz, J. A.; Troshin, P. A.; Gobsch, G.; Razumov, V. F.; Hoppe, H. Fullerene Solubility−Current Density Relationship in Polymer Solar Cells. *Phys. Status Solidi RRL* **2008**, *2*, 263−265.

(63) Susarova, D. K.; Goryachev, A. E.; Novikov, D. V.; Dremova, N. N.; Peregudova, S. M.; Razumov, V. F.; Troshin, P. A. Material Solubility Effects in Bulk Hetero Junction Solar Cells Based on the Bis-Cyclopropane Fullerene Adducts and P3HT. *Sol. Energy Mater. Sol. Cells* **2014**, *120*, 30−36.

(64) Kotlarski, J. D.; Blom, P. W. M. Impact of Unbalanced Charge Transport on the Efficiency of Normal and Inverted Solar Cells. *Appl. Phys. Lett.* **2012**, *100*, 013306/1−013306/3.

(65) Mihailetchi, V. D.; Xie, H.; de Boer, B.; Koster, L. J. A.; Blom, P. W. M. Charge Transport and Photocurrent Generation in Poly(3-hexylthiophene):Methanofullerene Bulk-Heterojunction Solar Cells. *Adv. Funct. Mater.* **2006**, *16*, 699−708.

(66) Blom, P. W. M.; Mihailetchi, V. D.; Koster, L. J. A.; Markov, D. E. Device Physics of Polymer:Fullerene Bulk Heterojunction Solar Cells. *Adv. Mater.* **2007**, *19*, 1551−1566.

(67) Troshin, P. A.; Susarova, K.; Khakina, E. A.; Goryachev, A. A.; Borshchev, O. V.; Ponomarenko, S. A.; Razumov, V. F.; Sariciftci, N. S. Material Solubility and Molecular Compatibility Effects in The Design of Fullerene/Polymer Composites for Organic Bulk Heterojunction Solar Cells. *J. Mater. Chem.* **2012**, *22*, 18433−18441.